Jurnal Teknologi

Full Paper

THE PROPERTIES OF SONICATED IMMERSION GROWN HEMATITE FILMS AT VARIOUS ANNEALING TEMPERATURES

Wan Rosmaria Wan Ahmad[a], Mohamad Hafiz Mamat[a,b*], Ahmad Sabirin Zoolfakar[a], Zuraida Khusaimi[b], Nur Izzah Khirul Ashar[a], N. Parimon[c], N. Vasimalai[d], I. B. Shameem Banu[d], Mohamad Rusop Mahmood[b]

[a]NANO-ElecTronic Centre (NET), School of Electrical Engineering, College of Engineering, Universiti Teknologi MARA, 40450 Shah Alam, Selangor, Malaysia
[b]NANO-SciTech Centre (NST), Institute of Science (IOS), Universiti Teknologi MARA, 40450 Shah Alam, Selangor, Malaysia
[c]Faculty of Engineering, Universiti Malaysia Sabah, 88400, Kota Kinabalu, Sabah, Malaysia
[d]School of Physical and Chemical Sciences, B.S. Abdur Rahman Crescent Institute of Science & Technology, Vandalur, Chennai 600 048, India

Article history
Received
16 November 2021
Received in revised form
15 June 2022
Accepted
25 July 2022
Published Online
31 October 2022

*Corresponding author
mhmamat@uitm.edu.my

Graphical abstract

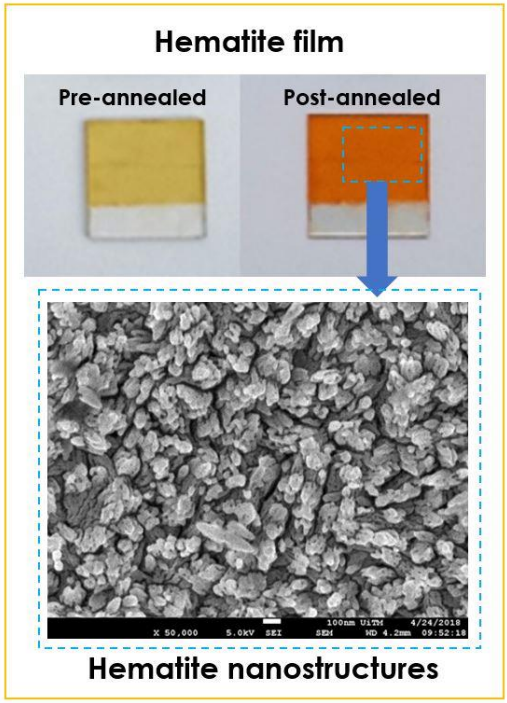

Abstract

In this research, hematite (a-Fe_2O_3) film was synthesised to study the effect of annealing temperature on its crystallinity, optical and electrical properties. Through a sonicated solution immersion technique, hematite films were deposited on a fluorine-doped tin oxide (FTO) glass substrate. In the synthesis process, 0.2 M ferric chloride ($FeCl_3 \cdot 6H_2O$) was used as a precursor, 0.2 M urea (NH_2CONH_2) as the stabilizer, and de-ionized (DI) water as a solvent to produce 200 ml of aqueous solution. During the annealing treatment, we varied the temperatures at 350 °C, 450 °C and 500 °C. The X-ray diffraction (XRD) pattern revealed the presence of peaks of 2θ angles between 20° to 90°, corresponding to (104), (110), (214), (125) and (128) planes, which exhibited crystalline structures of rhombohedral with diffraction peaks of hematite phase (a-Fe_2O_3). Optical characterisations showed that the transmittances of all samples were close to 100% in the high wavelength level of the visible light region, which is close to the infrared spectrum. Absorption of hematite samples was found to be more than 0.6 a.u. in the low wavelength level of the visible light region close to the ultraviolet spectrum and close to 0 in the high wavelength level of the visible light region close to the infrared spectrum. A sample with an annealing temperature of 500 °C has the lowest transmission and the highest absorbance in the visible region due to dim pigments in the hematite film. Electrical measurements have shown that the hematite samples have resistance values ranging from 13 to 62 Ω. Hematite samples annealed at 500 °C demonstrated suitable properties for humidity sensing applications.

Keywords: Hematite films, sonicated immersion, thermal annealing, annealing temperature, humidity sensing

Abstrak

Dalam penyelidikan ini, filem hematit (a-Fe_2O_3) telah disintesis untuk mengkaji kesan suhu sepuhlindap ke atas kehabluran, sifat optik dan elektriknya. Melalui teknik rendaman larutan sonikasi, filem hematit telah dimendapkan pada substrat kaca timah oksida (FTO) berdop fluorin. Dalam proses sintesis, 0.2 M Ferric Klorida ($FeCl_3 \cdot 6H_2O$) digunakan sebagai prekursor, 0.2 M urea (NH_2CONH_2) sebagai penstabil, dan air nyah-ion (DI) sebagai pelarut untuk menghasilkan 200 ml larutan akueus. Semasa rawatan sepuhlindap, kami mengubah suhu pada 350 °C, 450 °C dan 500 °C. Corak pembelauan X-ray (XRD) mendedahkan kehadiran puncak 2θ sudut antara 20° hingga 90°, yang sepadan dengan satah (104), (110), (214), (125) dan (128) yang mempamerkan struktur kristal rombohedral dengan puncak pembelauan fasa hematit (a-Fe_2O_3). Pencirian optik menunjukkan bahawa ketransmisian semua sampel menghampiri 100% pada tahap jarak gelombang tinggi di dalam cahaya tampak, yang menghampiri kepada spektrum inframerah. Penyerapan sampel hematit diperhatikan lebih besar daripada 0.6 a.u. di tahap jarak gelombang rendah di dalam cahaya tampak berhampiran dengan spektrum ultraungu dan menghampiri 0 di tahap jarak gelombang tinggi di dalam cahaya tampak berhampiran dengan spektrum inframerah. Sampel dengan suhu sepuhlindap 500 °C mempunyai transmisi yang paling rendah dan penyerapan yang paling tinggi di kawasan cahaya tampak disebabkan oleh pigmen malap dalam filem hematit. Pengukuran elektrik menunjukkan sampel hematit mempunyai nilai rintangan di dalam lingkungan 13 hingga 62 Ω. Sampel hematit yang disepuhlindap pada 500 °C menunjukkan sifat yang sesuai untuk aplikasi pengesanan kelembapan.

Kata kunci: Hematit, struktur nano, rendaman sonikasi, suhu sepuhlindap, pengesanan kelembapan

1.0 INTRODUCTION

In electronic devices nowadays, iron oxide is widely considered a versatile material as a sensing element for various applications. Development of the iron oxide framework has shown promising applications, including gas sensors [1], lithium-ion batteries [2], magnetic devices [3], and photocatalysts [4], and power water splitting [5]. The mineral compound of iron oxide is categorised based on their phases such as hematite (a-Fe_2O_3), magnetite (Fe_3O_4), and maghemite [6]. Among these three phases of iron oxide, pristine hematite (a-Fe_2O_3), is the most frequent polymorph. Hematite exists in nature as a mineral that can be found abundant in Earth's crust, rocks, and soils. Hematite typically comprises a higher iron content (by weight percent) of 70 % and only 30 % of oxygen. It is an n-type semiconductor compound in groups II-IV and exhibits the most stable phase of iron oxide under ambient conditions. In addition, hematite has wide band gap energy (E_g = 2.1 eV) and is simple to synthesise [7].

Hematite exhibits corundum type and rhombohedral structures which are made up of Fe^{3+} ions occupying two-thirds of the octahedral interstices in alternate layers, and an O^{2-} ion as a close-packed hexagonal crystallographic structure. Hematite is easier to synthesise than other polymorph phases of iron oxides as it is the end product of the iron oxide form of transformation, and it is extremely stable under environmental conditions. Hematite has been widely used for multiple applications in the semiconductor industry. It has produced the most important mineral compounds in the modern world [8].

Several techniques have been employed to synthesise hematite materials for sensor applications, such as sol-gel [9], hydrothermal [10], and spray pyrolysis [11]. Among these, the hydrothermal method is commonly being used to synthesise hematite materials, despite the requirement of high temperature, pressure, and long synthesis time. This process has produced hematite materials in form of granular particles to be applied in electronics applications. There are several parameters that could possibly affect the grown hematite film, for example the type of precursor and stabiliser used in the synthesis process [12], annealing treatments [13], and characteristics of substrate used in the synthesis. One of critical parameters to controlling the deposited hematite properties is the annealing treatment. In order to enhance the structure of the crystal lattice, the annealing treatment is necessary in the material synthesis process. In turn, this process improves the films' electrical properties as well as their adherence to the substrate [14]. Besides, the increasing annealing temperature would also have an impact on the growth of crystallite size, according to other studies on the annealing treatment based on various temperatures. [15, 16, 17]. However, it has been discovered that

extended annealing procedures have a negative impact on the crystallinity of hematite [18].

In this research, the effects of annealing treatments at various annealing temperatures on the structural as well as optical and electrical characteristics of hematite films were explored. The properties of hematite films were investigated based on varying annealing temperatures of 350 °C, 450 °C and 500 °C. The goal of this study is to improve the crystallinity of the hematite film by optimising the temperature via the annealing treatment for humidity sensing applications.

2.0 METHODOLOGY

In this research work, the sonicated immersion method was utilised to grow hematite layer on the substrate. The overall hematite development in this paper is separated into two main procedures, which are the synthesis of hematite and characterisation. The substrate was cleaned using a routine cleanings procedure before the synthesis stage. After the hematite preparation process was finished, annealing was applied to the prepared film to improve the crystal properties. The resulting film then investigated through a characterisation process.

2.1 Substrate Preparation

The fluorine-doped tin oxide coated glass substrate (FTO) was used for hematite synthesis. The dimension of the FTO was 2 cm × 2 cm. The conductive surface of the FTO has catalytic effect to facilitate the growth of nanostructured hematite film. Therefore, the FTO surface had to be free of impurities to ensure good quality hematite film formation. The cleansing was done during the substrate cleaning process. It began with sonicating the FTO substrates in Power Sonic 405 ultrasonic water bath (frequency: 40 kHz). The FTO was placed in a beaker filled with acetone for this process. Then, the sonication was conducted for 10 minutes at 50 °C. The substrates were washed thoroughly with DI water after sonication. Then, the sonication procedure was carried out once more in the beaker containing the FTO substrates by replacing the acetone with DI water. With the aim of drying the substrate, a nitrogen blowgun was used to remove water drops from the substrate surfaces. In order to prevent hematite growth, the tape was applied to a small section of the conductive surface of FTO after the substrate cleaning procedure was finished. This covered FTO area will serve as one of the electrodes for electrical measurement.

2.2 Synthesis Process

The synthesis was conducted based on our previous work [19], with some modifications were made for this experiment. Using a GR 200 analytical electronic balance, the weight of each material used in the synthesis of hematite was measured. All chemicals (i.e., precursor and stabiliser) were used as received without further purification. Both the precursor of ferric chloride ($FeCl_3 \cdot 6H_2O$) and the stabiliser of urea (NH_2CONH_2) were prepared as aqueous solutions in a beaker with a molarity of 0.2 M. The DI water was added until the final volume of the hematite precursor solution was 200 ml.

Then, the hematite precursor solution was sonicated for 30 minutes at 50 °C as shown in Figure 1(a). Sonication is required in this synthesis process to break the clustered materials apart for better reaction [17]. The sonicated hematite precursor solution was then stirred on the hotplate stirrer at room temperature with a speed=250 rpm for 5 minutes to achieve a homogeneous mixture, as shown in Figure 1(b).

Figure 1(c) illustrates the immersion procedure used to create hematite films. The conductive FTO layer was facing downward, and the FTO glass substrate was positioned parallel to and inside a precursor solution-filled Schott bottle before the immersion process. The Schott bottle was then inserted into the water bath apparatus shown in Figure 1 (d). The immersion process took 2 hours at 95 °C. The sample was drawn out of the Schott bottle and thoroughly washed with DI water after being submerged for 2 hours. The samples were then dried for 10 minutes at 150 °C as depicted in Figure 1(e).

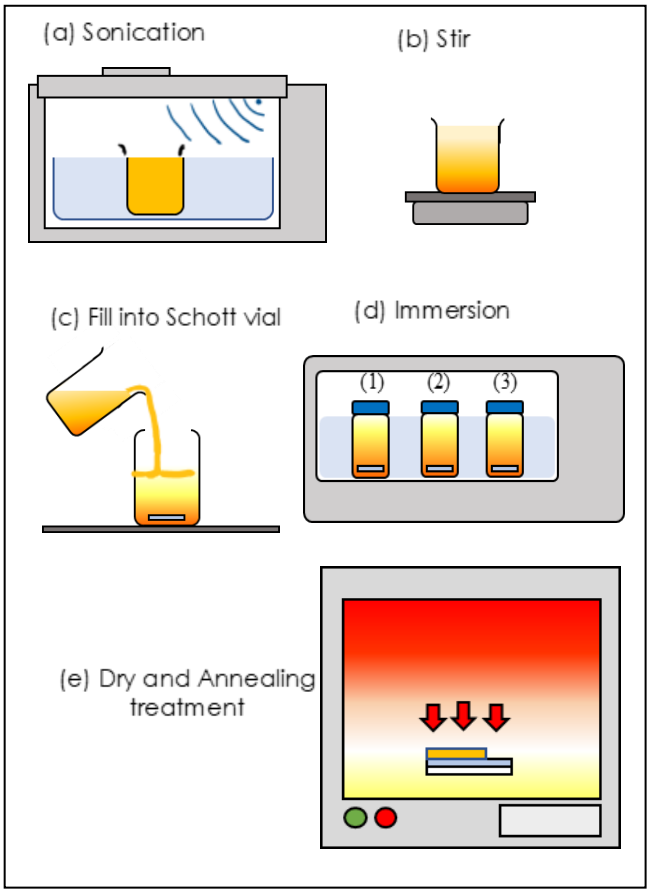

Figure 1 Synthesis process in sonication immersion method, (a) sonication, (b) stir, (c) fill the mixture solution and place the FTO-substrate in Schott vials, (d) immersion for three bottles of sample, and (e) drying and thermal annealing in a furnace

2.3 Annealing Treatment

The annealing process is essential for enhancing the crystalline nature of hematite films. After the sonication and immersion processes, the as-synthesized samples were annealed at 3 variations of temperature in a furnace (Protherm Furnaces). The samples were annealed separately for 1 hour at T = 350 °C, 450 °C, and 500 °C, as depicted in Figure 1(e). The samples annealed at T = 350 °C, 450 °C, and 500 °C were labelled as Sample A, Sample B, and Sample C, respectively. The samples were then cooled down to ambient temperature for characterisation.

2.4 Characterization

The properties of hematite films were characterised based on crystallinity, optical properties, and current-voltage (I-V) electrical characteristics as summarised in Figure 2(a). The photos for pre- and post-annealed samples were taken for comparison and macrostructural analysis. The morphology of the film was observed using JEOL field scanning electron microscope (FESEM). There were two samples prepared for each annealing temperature to facilitate different characterisation processes. One of the samples had no metal contact, as shown in Figure 2(b), which was used for material characterisation involving structural and optical properties. For metal contact purposes, silver (Ag) was deposited on another sample of hematite film using an electron beam thermal evaporator with a thickness of 60 nm, as shown in Figure 2(c). The sample with metal contact was used to measure the electrical I-V characteristics.

The synthesized dried samples were subjected to X-ray diffraction (XRD; PANalytical X'Pert PRO) with CuKa radiation (= 1.5406) at 2θ ranges from 10° to 90° operated at 30 kV and a scan speed of 2°/min for the crystallinity study. This characterisation was executed to analyse the crystallinity of the prepared hematite film that had grown on the FTO substrate. From the patterns made by XRD measurements, the results could be seen as diffraction peaks with different intensities.

For the optical characterisation, the samples were examined in terms of absorbance and transmittance characteristics using Varian Cary 5000 ultraviolet-visible (UV-Vis) spectroscopy. The degree of absorbance and transparency could be ascribed to the thickness and optical behaviour of the hematite film.

The I-V measurement with a dual probing system was executed within -5 V to 5 V, under ambient temperature and room illumination conditions. The compliance of the I-V measurement system was fixed at 100 mA. This measurement is essentially to analyse the electrical characteristics of hematite films. The sample probing set up is indicated as in Figure 3. The electrical measurement was conducted firstly using the contacts of deposited Ag and the FTO conductive layer, as shown in Figure 3 (*top*). Next, electrical measurement was performed by probing two Ag contacts as indicates in Figure 3 (*bottom*). The purpose of these measurements was to determine how different probe contacts influence electrical properties.

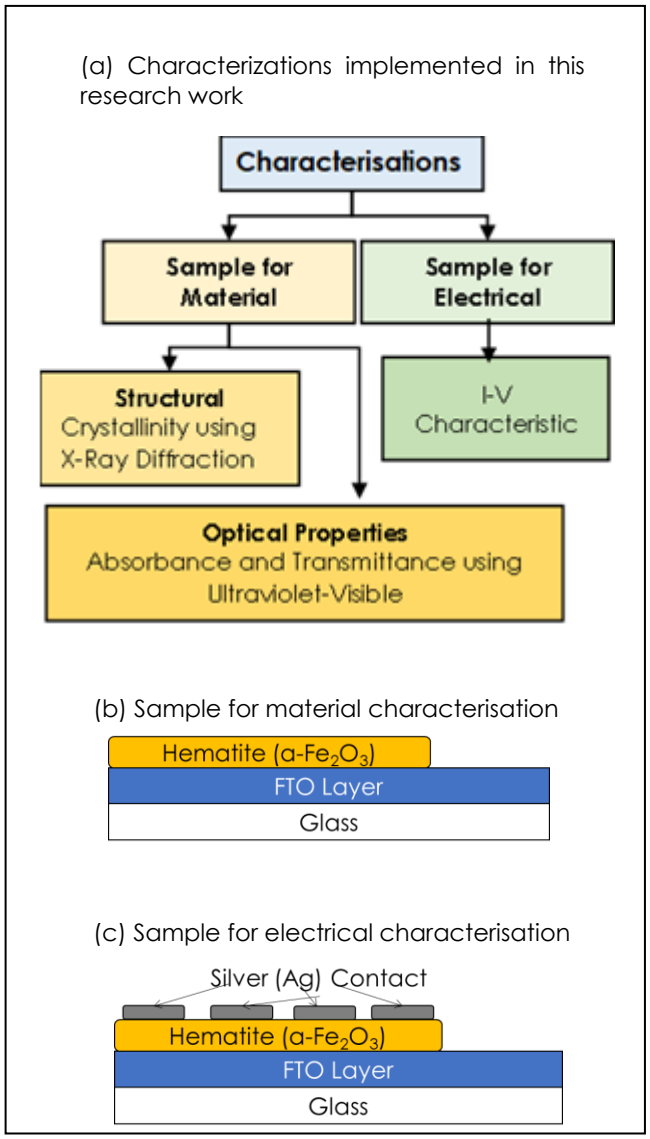

Figure 2 (a) Characterizations implemented in this work, (b) sample of grown hematite nanostructure film no metal contact, (c) sample with Silver (Ag) metal contact

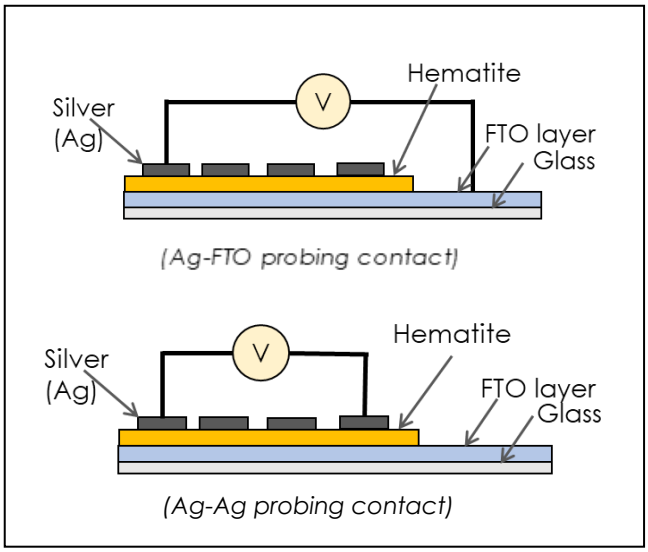

Figure 3 The electrical characterization probing set up, *(Ag-FTO)* probing contact (top), and *(Ag – Ag)* probing contact (bottom)

3.0 RESULTS AND DISCUSSION

The physical appearances of the grown hematite film for pre- and post-annealing treatments, as well as the FESEM images of the morphology of hematite nanostructure films for Samples A, B, and C, are shown in Figure 4. Figure 4 (left) illustrates the observation of the yellowish film pigment in all three pre-annealed samples using the same synthesis setup. The yellowish pigment became less intense in the post-annealing samples. Further investigation revealed that the post-annealed samples' film hues varied, as shown in Figure 4. (left). Sample A, which was annealed at 350 °C, has less intense pigments than sample C, which was annealed at 500 °C. This result suggests that annealing at a higher temperature increased the colour intensity of the hematite film. The increase in colour intensity can be attributed to the faster crystalline growth rate that occurred at a higher annealing temperature. [18]. An increase in annealing temperature also signifies a densification in the films that occurs during the annealing treatment, which is reflected in grain growth and coalescence [20].

The surface morphologies of the prepared hematite nanostructure samples at various annealing temperatures are shown in the FESEM image in Figure 4 (right), which was captured at a magnification of 50,000 x. All samples are seen to have nanorod structures distributed uniformly and grown perpendicular to the substrate surface. In contrast to the other samples, Sample C, which was annealed at 500 °C, exhibits large pores on the nanorods and a highly porous structure. The formation of pore areas between the nanorods may be caused by the evaporation of impurities during the annealing process and the merging activity of the nanorods at high temperatures. Hematite nanorods' average diameter sizes for Sample A (350 °C), Sample B (450 °C), and Sample C (500 °C) are estimated to be 55 nm, 76 nm, and 62 nm, respectively, according to measurements taken from the FESEM images.

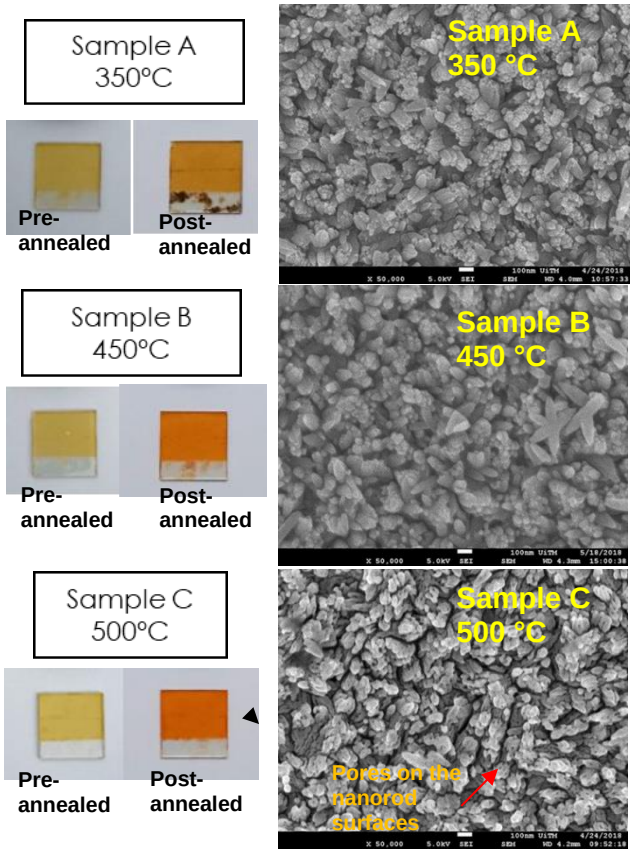

Figure 4 Physical appearance of hematite films pigments grown on FTO substrates after pre-annealing, and post-annealing (left), and the FESEM images showing the morphology of three samples, A, B, and C (right)

The XRD analyses of the synthesised samples for 350 °C (Sample A), 450 °C (Sample B), and 500 °C (Sample C) annealing temperatures revealed patterns as shown in Figure 5. Standard XRD data (JCPDS #33-00664) indicated that hematite films had a polycrystalline structure with a rhombohedral lattice structure based on the observed peaks of the hematite (α-Fe_2O_3) phase. Figure 5(a) shows the diffraction peaks of the hematite film and the FTO layer (from the substrate). Five hematite phase diffraction peaks, corresponding to the (104), (110), (214), (125), and (128) planes, were found at the following angles: 34.36°, 36.23°, 62.18°, 66.44°, and 81.37°, respectively.

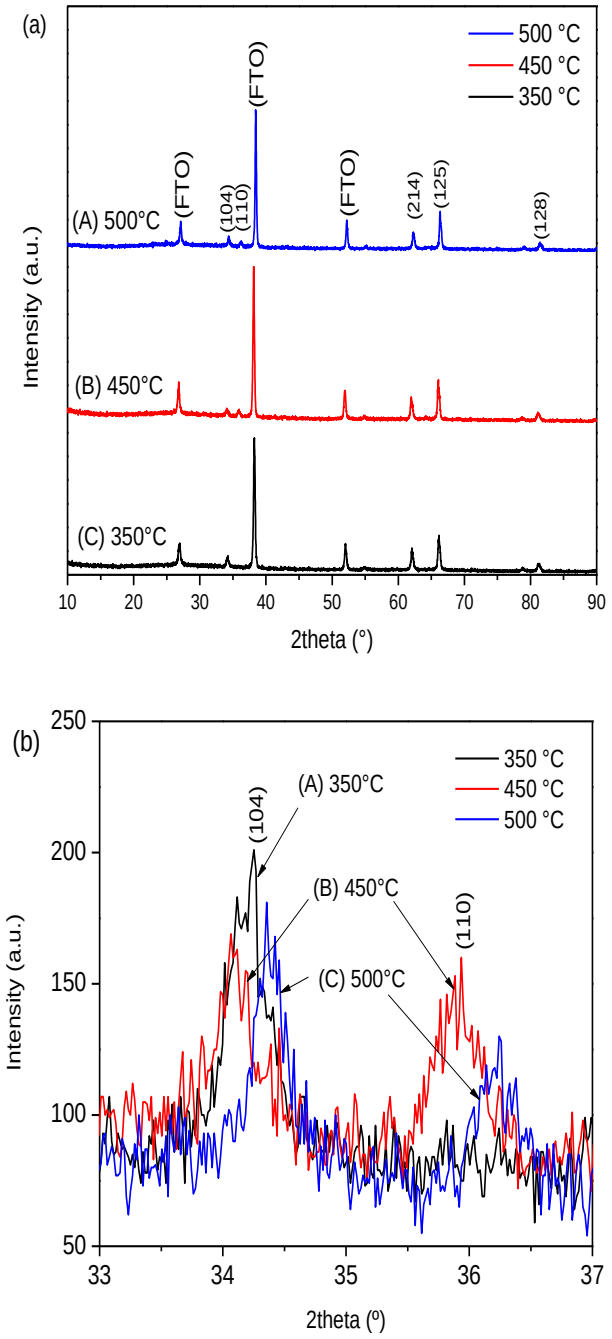

Figure 5 The crystallinity properties as exhibited by XRD pattern of hematite nanostructure films at various annealing temperatures (a) The XRD pattern in the ranges between 2θ=10° to 2θ=90°, (b) close-up diffraction peaks at 2θ between 33° to 37° shows that (110) plane does not appear in Sample A that annealed at 350°C

The high intensity of diffraction peaks at 26°, 38°, and 52° implies the property of the FTO conductive layer on the glass substrate which was not affected by the variation in annealing temperature. The FTO layer for all three samples likewise exhibits very large intensity diffraction peaks. Figure 5(b) displays the detailed diffraction peaks of the (104) and (110) planes for all three samples. The sample at the lowest annealing temperature (350 °C) does not exhibit the diffraction peak of the (110) plane, which is typically found between 35° and 37°. Hematite samples with annealing temperatures of 450 °C and 500 °C, on the other hand, showed diffraction peaks clearly at the (110) plane. This can be explained by the incomplete crystallisation process that occurred at a lower annealing temperature due to insufficient heat energy [16, 17]. It was also proven that annealing temperatures above or equal to 500 °C can completely convert γ-FeOOH to α-Fe_2O_3 [18]. Besides, the diffraction peak intensity of (110) or (104) in the synthesised samples also decreased with the increase of annealing temperature. The elevated annealing temperature had instigated the growth of hematite nanocrystals with crystallinity enhancement and the reduction of impurities that had formed a superior crystal in the hematite nanostructure film [19, 21].

The crystallite size, D, of the hematite nanostructure film was determined from the prominent peaks (104) and (110) by using the Debye-Scherrer formula [22]:

$$D = \frac{K\lambda}{\beta \cos\theta} \quad (1)$$

where λ is the wavelength used (1.5406 Å), β is the angular line width at half maximum intensity (FWHM) in radians, and θ is Bragg's angle. It is observed that the crystallite size of hematite Sample A is 4.9 nm, Sample B is 25.4 nm, and Sample C is 27.8 nm. This demonstrates that crystallite size does indeed increase with annealing temperature.

Furthermore, the total defects in the hematite films are determined by calculating the dislocation density, δ, using relation (2):

$$(\delta) = \frac{1}{D^2} \quad (2)$$

where D is the crystallite size of hematite nanostructure. According to the data compiled in Table 1, Sample A exhibits the highest density of dislocations, measuring at 412.78×10^{10} cm^{-2}. The dislocation density drops to 15.53×10^{10} cm^{-2} in sample B and 12.4×10^{10} cm^{-2} in Sample C as the annealing temperature rises. The micro strain, ε, of the deposited hematite nanostructure was determined from the following equation (3),

$$\varepsilon = \frac{\beta \cos\theta}{4} \quad (3)$$

where β is the FWHM and θ is Bragg's angle in radians. The micro strain, ε relates to the defect's presence around the hematite crystal lattice. Table 1 lists the variations of average diameter, crystallite size, dislocation density, micro strain, and electrical resistance for two probing configurations of deposited hematite at 350°C, 450°C, and 500°C of annealing treatment.

Table 1 The average diameter, crystallite size, dislocation density, micro strain, and electrical resistances of deposited hematite nanostructure films

Annealing Temperature (°)	(A) 350 °C	(B) 450 °C	(C) 500 °C
Average diameter size (nm)	55	76	62
Crystallite size, D (nm)	4.9	25.4	27.8
Dislocation density, δ (10^{10} cm^{-2})	412.8	15.5	12.4
Micro strain, ε (10^{-4})	73.6	14.3	12.8
Resistance, (Ω) (Ag-FTO)	41.04	61.95	58.53
Resistance, (Ω) (Ag-Ag)	33.27	13.81	26.36

The transmittance and absorbance of synthesised samples were measured in the range of wavelengths from 300 nm to 800 nm in the visible light range as demonstrated in Figure 6. According to the transmittance spectrum in Figure 6(a), the transmittance of all samples is greater than 80% for wavelengths ranging from 600 nm to 800 nm in the visible region. The spectra also show that Sample A, which was annealed to 350 °C, has the highest transmission for wavelengths less than 615 nm compared to the other two samples. Furthermore, at wavelengths ranging from 615 nm to 750 nm, Sample C, which was annealed at 500 °C, had the lowest transmission. This is probably due to dimmer pigments in the hematite films of samples with higher temperature annealing as reported in [23].

Referring to Figure 6(b), the absorbance of all hematite nanostructure film samples was found to be greater than 0.6 a.u. at wavelengths lower than 460 nm, closer to the ultraviolet spectrum, and approaching 0.0 a.u. at wavelengths higher than 600 nm. Sample C , which was annealed at the highest annealing temperature of 500 °C had a higher absorbance value at wavelengths ranging from 350 nm to 570 nm. This data is consistent with previous work by Marusak *et al.*, (1980) who reported a similar trend of absorption bands predicted by ligand field theory [24].

The absorbance bands from 500 to 800 nm wavelength are considered to arise from spin-forbidden ligand field transitions. The absorbance bands occurring between 400–500 nm are considered to arise from spin-flip transitions among the $2t_{2g}$ and $3e_g$ states, which have a higher intensity than spin-flip transitions, which are enhanced in materials with magnetic coupling [25]. The absorbance bands from 300–400 nm wavelength arise from O^{2-} to Fe^{3+} charge transfer between the *O* 2p nonbonding orbitals ($6t_{1u}$, $1t_{u}$) and the lowest empty orbital ($2t_{2g}\downarrow$). The lower wavelength features band (not shown in Figure 6(b)) are charge transfer transitions from O 2p nonbonding levels to the $3e_g$ orbital. As a result, those bands attribute the strongly absorbance characteristics of hematite (a-Fe_2O_3) in the visible and UV regions of the optical spectrum to allow transitions in origin that are either spin flip or charge transfer [24]. In this study, a large absorption coefficient is found to be accounted for by the charge transfer bands. From the transmittance and absorbance data, it is noted that hematite samples have a higher transmittance at higher wavelengths in the visible region close to the infrared spectrum, and a higher absorbance in the lower wavelengths close to the ultraviolet spectrum.

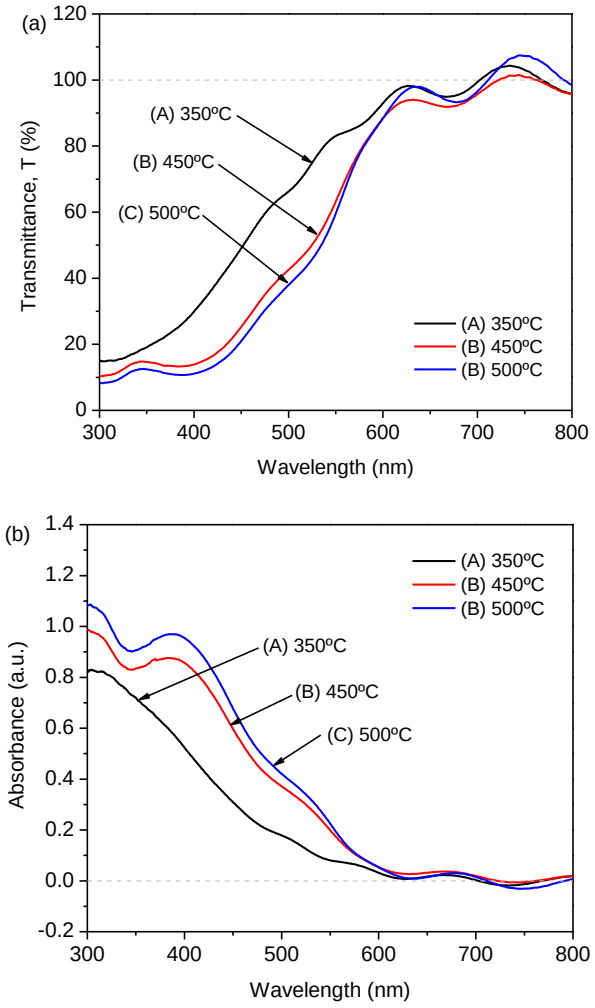

Figure 6 The optical properties of hematite nanostructure at different annealing temperatures, (a) transmittance, (b) absorbance

As the electrical characteristics of the Ag-FTO and Ag-Ag probing contacts were evaluated, it was discovered that the measurement through the Ag-FTO contact contributed to a steady behaviour, as shown in Figure 7(a). In this characteristic, hematite Sample B that is annealed at 450 °C shows the highest resistance (R=ΔV/ΔI), 61.95 Ω, followed by Sample C, annealed at 500 °C has resistance 58.53 Ω, and sample A, annealed at 350°C, 41.04 Ω, which has the lowest resistance as indicated in the Table 1. Meanwhile, Figure 7(b) depicts the electrical properties for the Ag-Ag contact measurement, which displays the ohmic response in all samples. Nonetheless, Sample B, which was annealed at 450 °C, has the lowest resistance as indicated in

Table 1 followed by Sample C and Sample A. As the resistance value only varies from 13 Ω to 33 Ω, the resistance values for all samples do not significantly differ from one another. A porous structure that was induced on the nanorod surfaces of Sample C, as shown in the FESEM image in Figure 4, may be the cause of the slightly higher resistance of Sample C compared to Sample B. It is possible for the porous surface to absorb oxygen molecules from the surrounding air, trapping carriers (such as electrons) in the process and creating adsorbed oxygen ions [26, 27]. As a result, the number of free electron carriers decreases, and the film's resistance rises. Meanwhile, previous work also reported that hematite films exhibit a high resistivity more than $>10^5$ Ωcm which indicates pure a-Fe_2O_3 characteristics [28]. It is expected that Sample C, which has a high density of pores on the nanorod surfaces, will produce a better sensor response because the resistance of the film is not noticeably different between Sample A, Sample B, and Sample C, and this hematite film fabrication is intended for humidity sensing applications.

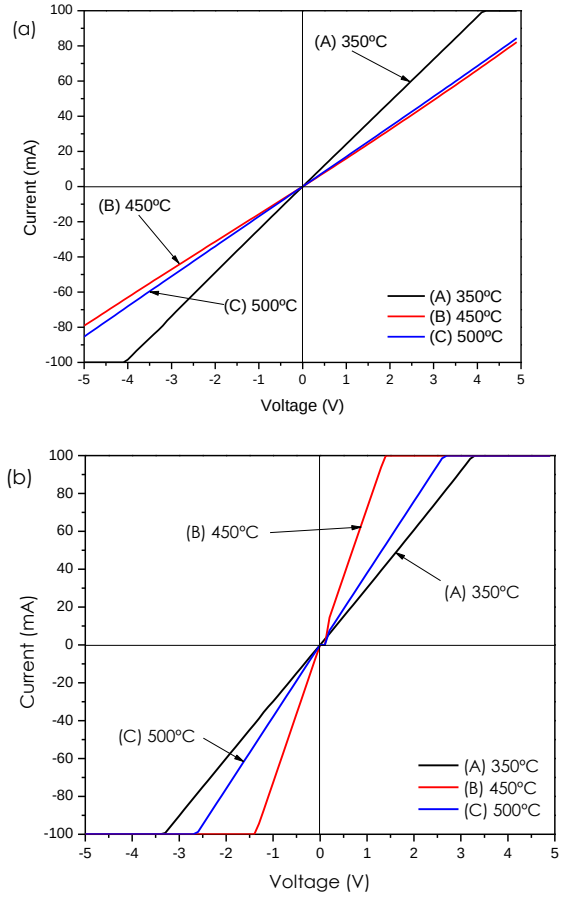

Figure 7 The electrical characteristics for hematite samples annealed at different temperatures based on (a) Ag-FTO contact and (b) Ag-Ag contact measurement

4.0 CONCLUSION

Hematite films were successfully prepared through the sonication immersion method for different annealing temperatures (350 °C, 450 °C, and 500 °C) to investigate the effect of increasing temperature during thermal annealing on the hematite structural, crystallinity, optical, and electrical properties. The XRD pattern has revealed rhombohedral structures of hematite crystals with diffraction peaks of hematite (a-Fe_2O_3) plane orientations. Sample A (350 °C), in contrast to samples B (450 °C) and C (500 °C), did not exhibit diffraction peaks in the (110) plane because the transition of the a-FeOOH goethite phase into the hematite (a-Fe_2O_3) phase was not complete. The nanorod structure of grown hematite, with an average size in the 50–80 nm range, was observed in FESEM images. While sample A's crystallite size is calculated to be 4.92 nm, samples B and C display crystallite sizes of 25.38 nm and 27.84 nm, respectively. In comparison to the other two samples (i.e., Sample B and Sample C), sample A has a much higher dislocation density (412.78×10^{10} cm^{-2}), indicating that the lattice has a higher number of defects. The hematite film samples were found to demonstrate high transmittance in the high wavelength region close to the infrared spectrum and high absorbance in the visible region close to the ultraviolet spectrum. Sample C, with an annealing temperature of 500 °C has the lowest transmission and the highest absorbance in the visible region, most likely due to dim pigments in the hematite nanostructure films. Sample C shows a slightly increased resistance value compared to Sample B due to the more porous surface posed by sample C. It is likely that Sample C, which was annealed at 500 °C, is the best sample for use in humidity sensing applications based on the structural, optical, and electrical data.

Acknowledgement

This work was supported by LESTARI grant (600-RMC/MYRA 5/3/LESTARI (012/2020)). The authors would like to acknowledge The Research Management Centre (RMC) UiTM, and Universiti Teknologi MARA (UiTM) for supporting the publication.

References

[1] Long, N. V., Teranishi, T., Yang, Y., Thi, C. M., Cao, Y., and Nogami, M. 2015. Iron Oxide Nanoparticles for Next Generation Gas Sensors. *International Journal of Metallurgical & Materials Engineering.* 1: 18. DOI: 10.15344/2455-2372/2015/119.

[2] Senthil, C., and Lee, C. W. 2020. Experimental Dataset on Tailoring Hematite Nanodots Embedded Nitrogen-rich Carbon Layers for Lthium-ion Batteries. *Data Brief.* 30: 105472. DOI: 10.1016/j.dib.2020.105472.

[3] Lassoued, A., Lassoued, M. S., Dkhil, B., Ammar, S., and Gadri, A. 2018. Synthesis, Structural, Morphological, Optical and Magnetic Characterization of Iron Oxide (a-Fe_2O_3) Nanoparticles by Precipitation Method: Effect of Varying the

Nature of Precursor. *Physica E: Low-dimensional Systems and Nanostructures.* 97: 328-334.
DOI: 10.1016/j.physe.2017.12.004.

[4] Carraro, G. *et al.* 2014. Nanostructured Iron(III) Oxides: From Design to Gas- and Liquid-phase Photo-catalytic Applications. *Thin Solid Films.* 564: 121-127.
DOI: 10.1016/j.tsf.2014.05.048.

[5] Tokubuchi, T., Arbi, R. I., Zhenhua, P., Katayama, K., Turak, A., and Sohn, W. Y. 2021. Enhanced Photoelectrochemical Water Splitting Efficiency of Hematite (α-Fe_2O_3)-Based Photoelectrode by the Introduction of Maghemite (γ-Fe_2O_3) Nanoparticles. *Journal of Photochemistry and Photobiology A: Chemistry.* 410.
DOI: 10.1016/j.jphotochem.2021.113179.

[6] Campos, E. A., Stockler Pinto, D. V. B., Oliveira, J. I. S. d., Mattos, E. D. C., and Dutra R. D. C. L. 2015. Synthesis, Characterization and Applications of Iron Oxide Nanoparticles - A Short Review. *Journal of Aerospace Technology and Management.* 7: 267-276.
DOI: 10.5028/jatm.v7i3.471.

[7] Tadic, M. *et al.* 2021. Rhombohedron and Plate-like Hematite (α-Fe_2O_3) Nanoparticles: Synthesis, Structure, Morphology, Magnetic Properties and Potential Biomedical Applications for MRI. *Materials Research Bulletin.*133.
DOI: 10.1016/j.materresbull.2020.111055.

[8] Najaf, Z. *et al.* 2021. Recent Trends in Development of Hematite (α-Fe_2O_3) as an Efficient Photoanode for Enhancement of Photoelectrochemical Hydrogen Production by Solar Water Splitting. *International Journal of Hydrogen Energy.* 46 (45): 23334-23357.
DOI: 10.1016/j.ijhydene.2020.07.111.

[9] Tongpool, R., Jindasuwan, S. 2005. Sol–gel Processed Iron Oxide–silica Nanocomposite Films as Room-temperature Humidity Sensors. *Sensors and Actuators B: Chemical.* 106(2): 523-528.
DOI: 10.1016/j.snb.2004.07.019.

[10] Tadic, M., Trpkov, D., Kopanja, L., Vojnovic S., and Panjan M. 2019. Hydrothermal Synthesis of Hematite (α-Fe_2O_3) Nanoparticle Forms: Synthesis Conditions, Structure, Particle Shape Analysis, Cytotoxicity and Magnetic Properties. *Journal of Alloys and Compounds.* 792: 599-609.
DOI: 10.1016/j.jallcom.2019.03.414.

[11] Henrist, C. *et al.* 2016. Surfactant-assisted Ultrasonic Spray Pyrolysis of Hematite Mesoporous Thin Films. *Microporous and Mesoporous Materials.* 221: 182-186.
DOI: 10.1016/j.micromeso.2015.09.046.

[12] Rehman, A., Zulfiqar, S., Shakir, I., Aly Aboud, M. F., Shahid, M., and Warsi, M. F. 2020. Nanocrystalline Hematite α-Fe_2O_3 Synthesis with Different Precursors and Their Composites with Graphene Oxide. *Ceramics International.* 46(6): 8227-8237.
DOI: 10.1016/j.ceramint.2019.12.050.

[13] Bedoya-Lora, F. E. *et al.* 2017. Effects of Low Temperature Annealing on the Photo-Electrochemical Performance of Tin-doped Hematite Photo-anodes. *Electrochimica Acta.* 251: 1-11.
DOI: 10.1016/j.electacta.2017.08.090.

[14] Carvalho-Jr, W. M. *et al.* 2019. Annealing Control of Hydrothermally Grown Hematite Nanorods: Implication of Structural Changes and Cl Concentration on Weak Ferromagnetism. *Journal of Alloys and Compounds.* 799: 83-88.
DOI: 10.1016/j.jallcom.2019.05.335.

[15] Mamat, M. H. *et al.* 2011. Controllable Growth of Vertically Aligned Aluminum-Doped Zinc Oxide Nanorod Arrays by Sonicated Sol–Gel Immersion Method depending on Precursor Solution Volumes. *Japanese Journal of Applied Physics.* 50(6).
DOI: 10.1143/jjap.50.06gh04.

[16] Pu, A., Deng, J., Hao, Y., Sun, X., and Zhong, J. 2014. Thickness Effect of Hematite Nanostructures Prepared by Hydrothermal Method for Solar Water Splitting. *Applied Surface Science.* 320: 213-217.
DOI: 10.1016/j.apsusc.2014.09.086.

[17] Phuan, Y. W., Chong M. N., Zhu, T., Yong, S.-T., and Chan E. S. 2015. Effects of Annealing Temperature on the Physicochemical, Optical and Photoelectrochemical Properties of Nanostructured Hematite Thin Films Prepared via Electrodeposition Method. *Materials Research Bulletin.* 69: 71-77.
DOI: 10.1016/j.materresbull.2014.12.059.

[18] Li, L., Zhang, H., Liu, C., Liang, P., Mitsuzaki, N., and Chen, Z. 2019. The Effect of Annealing Regime and Electrodeposition Time on Morphology and Photoelecrochemical Performance of Hematite Converted from Nanosheet γ-FeOOH. *Journal of Photochemistry and Photobiology A: Chemistry.* 369: 8-15.
DOI: 10.1016/j.jphotochem.2018.10.005.

[19] Ahmad, W. R. W., Mamat, M. H., Khusaimi, Z., Ismail, A. S., and Rusop, M. 2019. Impact of Annealing Temperature to the Performance of Hematite Based Humidity Sensor. *Indonesian Journal of Electrical Engineering and Computer Science.* 13(3).
DOI: 10.11591/ijeecs.v13.i3.pp1079-1086.

[20] De Souza L. P., Chaves, R. O. G., Malachias, A., Paniago, R., Ferreira, S. O., and Ferlauto, A. S. 2016. Influence of Annealing Temperature and Sn Doping on the Optical Properties of Hematite Thin Films Determined by Spectroscopic Ellipsometry. *Journal of Applied Physics.* 119(24).
DOI: 10.1063/1.4954315.

[21] Soleimani, H. *et al.* 2014. Effect of Annealing Temperature on the Crystallization of Hematite-Alumina (Fe_2O_3-$Al2O_3$) Nanocomposite and its Influence in EOR Application. *Journal of Nano Research.* 29: 105-113.
DOI:10.4028/www.scientific.net/JNanoR.29.105.

[22] Ubale, A. U. and Belkhedkar M. R. 2015. Size Dependent Physical Properties of Nanostructured α-Fe_2O_3 Thin Films Grown by Successive Ionic Layer Adsorption and Reaction Method for Antibacterial Application. *Journal of Materials Science & Technology.* 31(1): 1-9.
DOI: 10.1016/j.jmst.2014.11.011.

[23] Wang, J., White W. B., and Adair, J. H. 2005. Optical Properties of Hydrothermally Synthesized Hematite Particulate Pigments. *Journal of the American Ceramic Society.* 8(12): 3449-3454.
DOI: 10.1111/j.1551-2916.2005.00643.x.

[24] Marusak, L. A., Messier, R., William B., White, 1980, Optical Absorbtion Spectrum of Hematite, α-Fe_2O_3 Near IR to UV. *Phys. Chem. Solids.* 41: 981-984.
DOI:10.1016/0022-3697(80)90105-5.

[25] Trpkov, D., Panjan, M., Kopanja, L., and Tadić, M. 2018. Hydrothermal synthesis, Morphology, Magnetic Properties and Self-assembly of Hierarchical α-Fe_2O_3 (Hematite) Mushroom-, cube- and Sphere-like Superstructures. *Applied Surface Science.* 457: 427-438.
DOI: 10.1016/j.apsusc.2018.06.224.

[26] Mamat, M. H. *et al.* 2022. Heterojunction of SnO_2 Nanosheet/arrayed ZnO Nanorods for Humidity Sensing. *Materials Chemistry and Physics.* 288: 126436.
DOI: https://doi.org/10.1016/j.matchemphys.2022.126436.

[27] Ismail, A. S. *et al.* 2018. Heterogeneous SnO2/ZnO Nanoparticulate Film: Facile Synthesis and Humidity Sensing Capability. *Materials Science in Semiconductor Processing.* 81: 127-138.
DOI: https://doi.org/10.1016/j.mssp.2018.03.022.

[28] Glasscock, J. A., Barnes, P. R. F., Plumb, I. C., Bendavid, A., Martin, P.J. 2008. Structural, Optical and Electrical Properties of Undoped Polycrystalline Hematite Thin Films Produced using Filtered Arc Deposition. *Thin Solid Films.* 516(8): 1716-1724.
DOI: https://doi.org/10.1016/j.tsf.2007.05.020.